Development of nanomaterial enabling highly sensitive SALDI-MS peptide analysis

Aline Cournut, Ioana Silvia Hosu, Flavie Braud, Paul Moustiez, Yannick Coffinier, Christine Enjalbal, Claudia Bich

Received: 14 December 2022 | Revised: 14 January 2023 | Accepted: 18 January 2023

DOI: 10.1002/rcm.9476

RESEARCH ARTICLE

Rapid Communications in Mass Spectrometry WILEY

Development of nanomaterial enabling highly sensitive surface-assisted laser desorption/ionization mass spectrometry peptide analysis

Aline Cournut[1] | Ioana Silvia Hosu[2] | Flavie Braud[3] | Paul Moustiez[3] | Yannick Coffinier[3] | Christine Enjalbal[1] | Claudia Bich[1]

[1]Univ. Montpellier, CNRS, ENSCM, IBMM, UMR 5247, Montpellier, France

[2]Bioresources Department, National Institute for Research and Development in Chemistry and Petrochemistry, Bucharest, Romania

[3]Univ. Lille, CNRS, UMR 8520 - IEMN, Lille, France

Correspondence
C. Bich, Univ. Montpellier, CNRS, ENSCM, IBMM, UMR 5247, Montpellier, France.
Email: claudia.muracciole-bich@umontpellier.fr

Funding information
Agence Nationale de la Recherche, Grant/Award Numbers: ANR NanoIntra ANR-19-CE09-0030, ANR-11-EQUIPEX-0025; Centre National de la Recherche Scientifique (CNRS); University of Lille; University of Montpellier; RENATECH

Rationale: Surface-assisted laser desorption/ionization mass spectrometry (SALDI-MS) is an approach derived from matrix-assisted laser desorption/ionization (MALDI)-MS which overcomes the drawbacks associated with the use of organic matrices required to co-crystallize with the analytes. Indeed, nanomaterials commonly used in SALDI-MS as inert surfaces to promote desorption/ionization (D/I) ensure straightforward direct deposition of samples while providing mass spectra with ions only related to the compound of interest. The objective of this study was to develop a novel SALDI-MS approach based on steel plates that are surfaces very rapidly and easily tuned to perform the most efficient peptide detection as possible. To compare the SALDI efficacy of such metal substrates, D/I efficiency and deposit homogeneity were evaluated according to steel plate fabrication processes.

Methods: The studied surfaces were nanostructured steel plates that were chemically modified by perfluorosilane and textured according to different frequencies and laser writing powers. The capacity of each tested 100 surfaces was demonstrated by comparative analyses of a mixture of standard peptides (*m/z* 600–3000) performed with a MALDI-TOF instrument enabling MALDI, SALDI and imaging experiments.

Results: A peptide mix was used to screen the different surfaces depending on their D/I efficiency and their ability to ensure homogeneous deposit of the samples. For that purpose, deposition homogeneity was visualized owing to reconstructed ionic images from all protonated or sodiated ions of the 10 peptides constituting the standard mix.

Conclusions: Seven surfaces were then selected satisfying the required D/I efficiency and deposit homogeneity criteria. Results obtained with these optimal surfaces were then compared with those recorded by MALDI-MS analyses used as references.

1 | INTRODUCTION

Established in the late 1960s, laser desorption/ionization mass spectrometry (LDI-MS)[1,2] has become a powerful analytical tool over the years for various applications such as macromolecule or small-molecule detection. More specifically, matrix-assisted laser desorption/ionization (MALDI), which was introduced by Karas and Hillenkamp in the late 1980s,[3] is widely used as one of the most advanced and sensitive MS technologies.[4] This technique uses an organic matrix which co-crystallizes with the analyte of interest to enable desorption/ionization (D/I) phenomena. MALDI matrices must absorb at the laser wavelength to be efficient. Most common ones, regarding peptide and protein analysis, are α-cyano-4-hydroxycinnamic acid (CHCA), 2,5-dihydroxybenzoic acid (DHB) and sinapinic acid.[5–8] MALDI-MS is used for applications in screening and diagnostic research or for the characterization of synthetic polymers and biopolymers. Moreover, clinical microbiology applies this technique for identification of toxins and microorganisms. MALDI-MS is also used by chemical analysts and biomedical researchers or for studying macromolecules.[9–14] Although MALDI analysis offers many advantages, the addition of a small organic compound as matrix involves several issues. The presence of the matrix with the sample negatively impacts the analysis in the low-mass region. Indeed, it causes a high background noise. Moreover, the co-crystallization process leads to a lack of reproducibility due to the presence of "hot spots" at the surface of the sample.[15] Such an occurrence can be specifically evidenced using MS imaging (MSI) analysis. MSI then makes it possible to evaluate the spot homogeneity.[16–19] Regarding those drawbacks, multiple MALDI derived techniques have emerged over the years. Among them, inorganic substrates investigated as alternative matrices led to so-called surface-assisted laser desorption/ionization (SALDI)-MS whose terminology was proposed in 1995 by Sunner and co-authors.[20] The first SALDI-related technology was introduced by Tanaka et al in 1988 who used ultrafine cobalt nanopowders mixed with glycerol matrix to analyze peptides and proteins of up to 20 kDa.[21] Even though such a strategy counted on a mixed system (organic/inorganic) to produce ions, it paved the way to the use of solely inert material to perform efficient LDI analyses. Since then, SALDI-MS has been one technique, among many, dedicated to analysis of small molecules and macromolecules. For the past 20 years, multiple structured materials have been developed for SALDI-MS analysis.[22,23] The substrates can be from various origins such as metallic-based, carbon-based or silicon-based nanostructures, as well as quantum dots or metal–organic frameworks. Nanosubstrates need specific characteristics to assist the LDI process, such as strong absorption in the UV range, a low heat capacity and a large surface area per unit volume.[24] Moreover, SALDI nanosubstrates have significant advantages compared to classic MALDI organic matrices such as low chemical background on mass spectra and their high molecular loading capacities.[25,26] Although some nanomaterials are known for their affinity for specific functional groups which can be used to specifically analyze certain classes of analytes,[27,28] one of the most important parameters is the nanosubstrate morphology. Indeed, the type of nanostructure, the porosity, the roughness, the size or even the pore depth can significantly affect the efficiency of the D/I process.[29–31] For instance, the higher the porosity of the substrate, the lower the threshold of the laser must be whereas the pore size and the interpore spacing do not have much impact. The laser threshold also decreases when the surface voidage is increasing and the substrate has higher optical absorption. Many research areas have been relying on nanosubstrates in SALDI-MS and SALDI-MSI analysis such as pharmaceuticals research,[32,33] biomedicine,[34,35] molecular biology,[36] environmental science[37] and forensics.[38] For instance, SALDI-MS has been conducted to identify three 4-methylenedioxymethamphetamine impurities using a specific nanosubstrates based on porous silicon allowing one to trace back the origin of dope pills.[39] It has also been used to detect nonsteroidal anti-inflammatory drugs and dyes in water samples with an Au–TiO_2 nanohybrid substrates.[40] A novel SALDI approach was used to detect methadone from spiked saliva and clinical urine samples.[41] Liu and coworkers also proposed in 2017 new hydroxyl-group-dominated graphite dots for biomolecule analysis. In that study, puerarin metabolite distribution in a mouse kidney was shown with the use of MSI experiments.[42]

Even though SALDI-MS has many advantages for peptide analysis, it is crucial to improve its detection sensitivity to a level comparable to that of MALDI-MS. Moreover, the finding of a universal matrix (organic or inorganic) is still ongoing. The objective here is to develop a SALDI-MS approach based on steel plate substrates enabling rapid, easy and highly sensitive detection of peptides. Indeed, steel plate surfaces are straightforward to fabricate and convenient to use as SALDI substrates. Such surfaces can thus provide an inorganic matrix with endless possibilities of MS analyses for a wide range of compounds. In the work reported in this article, we aimed at designing structured steel surfaces dedicated to the analyses of biomolecules with performances equaling that of MALDI methodology which was taken as reference for SALDI-MS validation. For that purpose, the efficiency of D/I was firstly optimized on a reference peptide mix deposited onto the SALDI steel plates to select the best ones. Secondly, deposit homogeneity was probed for a few selected surfaces using MSI mode. Finally, selection of the best SALDI steel substrates according to both their D/I efficiency and sample homogeneity was made and validated with MALDI-MS results.

2 | EXPERIMENTAL

2.1 | Chemicals

MALDI matrices (CHCA, DHB), trifluoroacetic acid (TFA) as well as acetonitrile (ACN) and water of HPLC grade were purchased from Sigma-Aldrich (St Louis, MO). The peptides used as references in the standard mixtures were prepared according to conventional solid-phase protocols and purified by preparative reversed-phase HPLC.[43,44]

2.2 | Steel plate fabrication

Arrays of 100 surfaces of 9 mm^2 each were prepared on two plates that were differently patterned. Steel plate #1 contained 50 positions chemically modified with perfluorosilane and subjected to a single laser writing with a horizontal hatch pattern defined as follows: written frequencies of 10, 50, 100, 150 and 200 kHz and laser powers ranging from 10% to 100%. Steel plate #2 contained also 50 surfaces prepared similarly but with 10 laser passes. The writing speed was 75 mm s^{-1} and the writing pitch was 35 µm for each surface of the two steel plates. The steel plates were textured with an Oxford Lasers E series (Femtosecond) at 1064 nm.

2.3 | Sample preparation

CHCA and DHB matrices were used as received without recrystallization. CHCA and DHB matrix solutions were daily prepared at 10 and 50 mg mL^{-1} respectively, in H_2O/ACN/TFA (30/70/0.1). Peptide solutions were prepared at 1 mg mL^{-1} in H_2O/ACN/TFA (30/70/0.1). For the standard peptide mix described in Table 1 ("peptide 10 reference mix"), each of the peptide solutions was mixed and diluted to a final concentration of 83 mg L^{-1} with the same solvent.

2.4 | LDI-MS analysis

LDI mass spectra were recorded with a Rapiflex instrument (Bruker Daltonics, Wissembourg, France). A smartbeam pulsed Nd:YAG laser at a wavelength of 355 nm was operated at a frequency of 10 kHz with a delayed extraction time of 160 ns. An acceleration voltage of 20 kV was applied and the reflectron mode was used. The source was operated in the positive ion mode. Data were acquired with FlexControl 4.0 software and processed with FlexAnalysis 4.0 software. Imaging data were processed with FlexImaging 5.0 software. For MALDI analyses, a pre-mix solution of 10 µL of matrix solution with 4 µL of the peptide solution was made prior to deposition of 0.5 µL according to the dried droplet procedure. For SALDI analyses, the deposition volume was restricted to 2 µL of the sample solution directly deposited onto the steel plate surfaces. All MALDI-MS acquisitions were performed in the "Custom" mode, with a laser fluence set at 60% and number of shots of 1000 with five spectra additions. All SALDI-MS acquisitions were performed in the "MS Dried Droplet" mode, with a laser fluence set at 90% and number of shots of 1000 with five spectra additions. Applied laser fluences correspond to relative values of a preselected confined range of the software. Number of shots was set at 300 instead of 1000 for all MSI analysis. The laser acquisition pattern was optimized according to MALDI or SALDI acquisitions as presented in Section 3. MSI experiments were conducted with spatial resolution of 25 × 25 $µm^2$ and of 84 × 84 $µm^2$ for MALDI and SALDI technologies, respectively.

3 | RESULTS AND DISCUSSION

The reliability and ease of fabrication of steel plates make them very attractive ready-to-use SALDI surfaces. In order to position such SALDI substrates versus conventional MALDI-MS analyses, the latter were first optimized to serve as reference prior to actual SALDI-MS method development on the variety of prepared steel plates.

3.1 | MALDI-MS analysis optimization for peptide data acquisition reference protocols

First of all, several organic matrices were tested and compared for their comprehensive detection of a reference peptide mixture containing 10 synthetic sequences. These peptides were selected to present different physicochemical properties and covered a mass range from 500 to 3000 Da as displayed in Table 1. Among all possibilities, CHCA, which is the most-used matrix for peptide analysis, and DHB, which is alternatively employed, were chosen.[5,6] Figure 1 presents the mass spectra obtained for the analysis of the reference mixture containing 10 peptides with CHCA matrix (Figure 1A) and DHB matrix (Figure 1B). Under optimal conditions

TABLE 1 Composition of the standard peptide mix

Peptide no.	Sequence	Monoisotopic mass (u)	$[M + H]^+$	$[M + Na]^+$
1	VTEFQ	622.2962	623.3035	645.2855
2	LAVGIAR	698.4439	699.4512	721.4331
3	FPCEAFA	783.3262	784.3334	806.3154
4	GFTWGVAGY	956.4392	957.4465	979.4284
5	AFAMVGKLAE	1035.5423	1036.5496	1058.5315
6	PGAHIWEAGAK	1135.5774	1136.5847	1158.5667
7	CLYEFAFISVGPLAR	1684.8647	1685.8720	1707.8539
8	CLVAHIGSWVAAWAYGIPVIHVGR	2574.3682	2575.3755	2597.3574
9	IGLAGWIVFAPIGLVWFAGLPVIAR	2635.5407	2636.5479	2658.5299
10	FHNGLIFMFAFAPLVHIWEAGAPLR	2853.4941	2854.5014	2876.4833

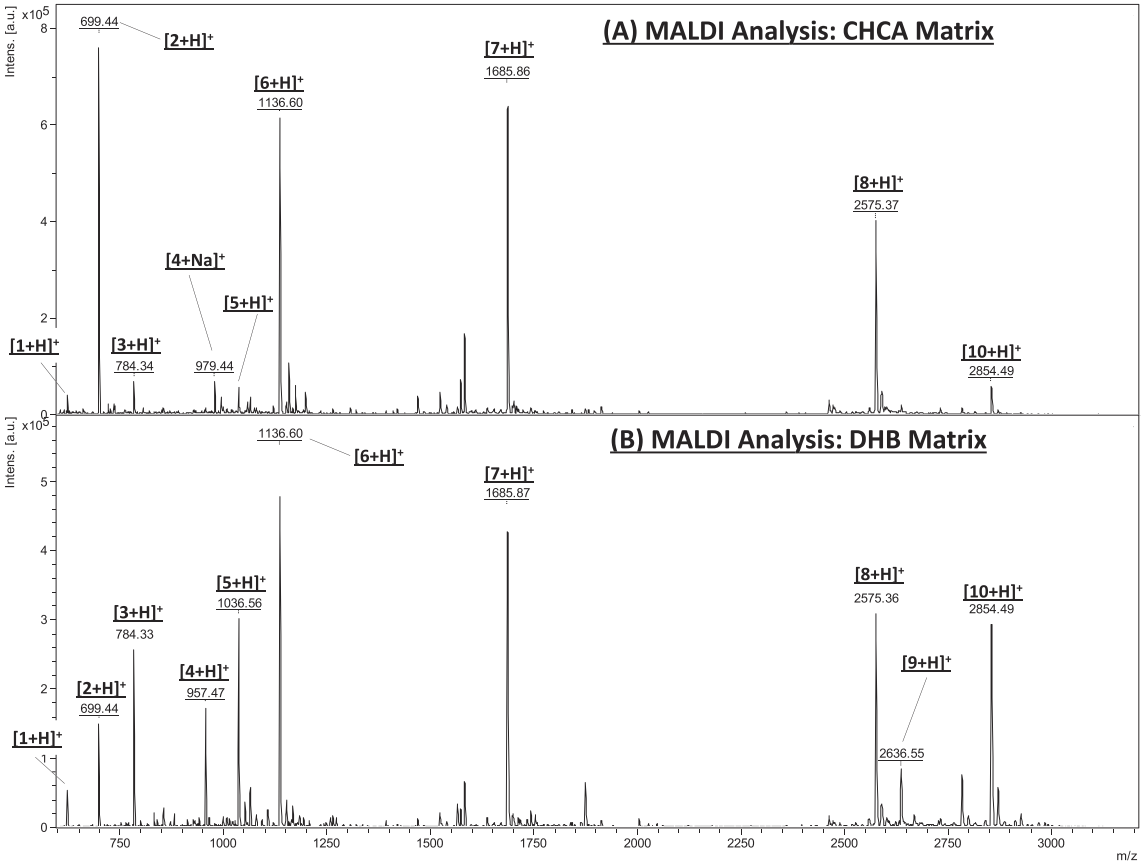

FIGURE 1 MALDI-MS spectra of the reference peptide mixture performed in positive mode with (A) CHCA matrix and (B) DHB matrix

(laser fluence, sample concentration, matrix-to-sample ratio, etc.), the identification of nine out of the ten sequences was achieved with the CHCA matrix. Surprisingly, the DHB matrix provided better results allowing the detection of all ten peptides of the mixture with an improved sensitivity. Indeed, after comparison between CHCA and DHB conditions of all defined performance criteria (area, intensity and signal-to-noise ratio as presented in Table S1 of the supporting information), it was noticeable that the DHB matrix was by far more efficient than CHCA. Another important fact to note is that peptides were ionized under three predominant forms, producing hydrogen, sodium and potassium adducts (H^+, Na^+ and K^+). While the CHCA matrix provided all ionization states, the DHB matrix favored the protonated ions (H^+ forms) that were predominant in the spectra. Detection sensitivity was thus enhanced in such a case gathering all peptide ions under a single signal. Nevertheless, selection of the optimal matrix does not only rely on D/I efficiency. Indeed, one of the major drawbacks of MALDI-MS is the inability of the matrix and the sample to co-crystallize in a homogeneous way leading to the peptides mostly being concentrated on "hot spots" or on the edges of the dried droplet ("coffee stain effect").[15,16,45–49] Hence, MALDI-MS imaging experiments have been realized with the studied peptides to optimize the protocol by adapting the volume of deposit, the matrix-to-sample ratio, the matrix concentration and the solvent. As expected, deposits performed with DHB, which is known to co-crystallize with crystal-shape needles, showed poor homogeneity leading to no reproducible analyses, whereas CHCA behaved far better as depicted in Figure S1 of the supporting information. Furthermore, to overcome the "hot-spot" issue, another experimental parameter related to instrumental settings was also investigated. Hence, the laser irradiation path followed during the analysis can be optimized to hit the whole sample surface. Dealing with dried droplet deposits or inert substrates, such issue is of particular importance to achieve efficient analysis deserving specific attention. For that purpose, all automated prerecorded laser acquisition patterns, already available with FlexControl software, were tested (see Table S2 of the supporting information). In addition, several "in-house" pathways were also created (using Excel and Notepad++ software). Three of the 17 prerecorded laser acquisition patterns were firstly selected according to their theoretical number of shots and physical movement on the target. These selected methods (called "Hexagon," "5" and "Walk On Spot") were then compared under MALDI conditions. To do so, 23 deposits were made on a MALDI plate using two matrices (CHCA and DHB) and three different peptide mixes. The consecutive analyses of those 23 spots with each of the above-mentioned methods were made (data not shown). Method 5 was the least efficient only allowing the detection of the peptide mix in 14 spots. On the other hand, Hexagon and Walk On Spot methods allowed the detection of the mixtures in 22 and 21 spots, respectively. The Walk

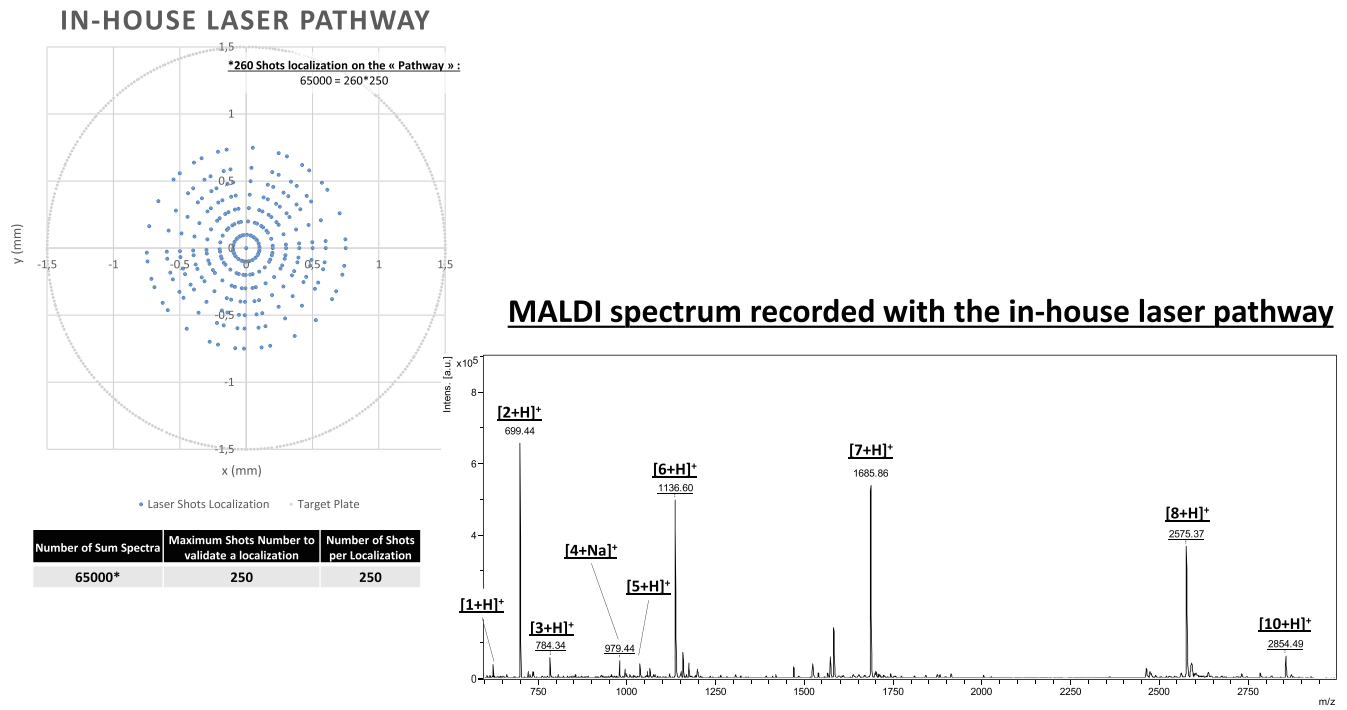

FIGURE 2 Optimal in-house automated laser acquisition pattern scheme and corresponding MALDI-MS spectrum of the reference peptide mixture obtained in positive mode with CHCA matrix [Color figure can be viewed at wileyonlinelibrary.com]

On Spot method parameters cannot be changed or further optimized with FlexControl software. For that reason, four in-house pathways were created on the basis of the alterable Hexagon method. The left-hand panel of Figure 2 shows the optimal in-house laser acquisition pattern operating on a single target spot. In the right-hand panel, one of the mass spectra recorded with this laser acquisition pattern from the reference peptide mixture is displayed. Only one in-house laser acquisition pattern of four showed expected and efficient results meaning that peptides from the mix were always detected on the target with this method. According to all described investigations, despite the better peptide coverage and detection sensitivity obtained with DHB, the CHCA matrix was preferred due to its greater deposit homogeneity. For this reason, the reference MALDI spectra were recorded with the CHCA matrix associated with the customized Hexagon laser irradiation method.

3.2 | SALDI-MS analyses for evaluation of most appropriate steel plate preparation protocol

Once MALDI-MS reference spectra had been selected after thorough acquisition method optimization, spectra were then recorded with the SALDI substrates of interest according to the previously defined customized laser acquisition pattern. Comparison of datasets allowed selecting the best prepared steel plates for subsequent further refining of preparation protocols and concomitant SALDI-MS tuning. Indeed, these nanostructured surfaces were first chemically modified with perfluorosilane and then textured with a laser according to various parameters governing the photon beam which included power, direction (vertical and/or horizontal), speed of writing as well as number of passages. Considering the 100 different studied surfaces originating from diverse texturing conditions, three criteria were scrutinized to probe their respective SALDI-MS behaviors: the contact angle of the deposit related to the facility of sample deposition; the D/I efficiency to achieve sensitive detection; and the homogeneity of the deposits to provide insights on the quality of substrate sample coverage. To probe these items directly linked to the overall analysis performance, the same mixture of 10 reference peptides used for MALDI-MS was deposited on the variety of prepared steel plates.

3.2.1 | Contact angle

The contact angle of each surface, and therefore its hydrophobicity, was found dependent on the laser writing parameters. The higher the writing laser frequencies and powers were, the more difficult was the deposition step. In the same way, surface patterns of the steel plate with one laser passage (steel plate #1) were less hydrophobic than those obtained after 10 passages (steel plate #2). So, optimal contact angles that were evaluated between 120° and 150° enabled straightforward sample deposition. Above 150°, the surfaces were too hydrophobic to allow any deposition. Taking into account that the reference peptide mixture was conditioned in water as sole solvent, the peptide mixture was diluted with a solvent containing 70% of ACN in order to overcome this issue. Adding such an organic solvent

FIGURE 3 SALDI-MS steel plate #1 (left-hand column) and steel plate #2 (right-hand column) D/I efficiency results obtained for the reference peptide mix analysis with MS Dried Droplet mode. (A) Areas under the peaks observed for each peptide molecular ion for the whole mixture deposited on (A#1) steel plates #1 and (A#2) steel plates #2. (B) Areas under the peaks observed for peptides 2 and 9 molecular ions deposited on (B#1) steel plates #1 and (B#2) steel plates #2. (C) Areas under the peaks observed for peptides 6, 7 and 10 molecular ions deposited on (C#1) steel plates #1 and (C#2) steel plates #2. (D) Areas under the peaks observed for peptides 1, 4 and 5 molecular ions deposited on (D#1) steel plates #1 and (D#2) steel plates #2 [Color figure can be viewed at wileyonlinelibrary.com]

TABLE 2 Optimal writing laser powers and frequencies for each peptide group deposited on steel plate #2

		Selected surfaces from two acquisition modes			
		MS Dried Droplet mode		Custom mode	
	Peptide groups	Writing laser power (%)	Writing laser frequency (kHz)	Writing laser power (%)	Writing laser frequency (kHz)
No.	Sequence	P	F	P	F
2 9	LAVGIAR IGLAGWIVFAPIGLVWFAGLPVIAR	100	50	–	–
		100	**10**	**100**	**10**
		–	–	90	10
		80	10	80	10
		70	**10**	**70**	**10**
		–	–	60	10
		50	10	–	–
		–	–	40	10
		–	–	10	100
		10	**150**	**10**	**150**
		–	–	10	200
6 7 10	PGAHIWEAGAK CLYEFAFISVGPLAR FHNGLIFMFAFAPLVHIWEAGAPLR	**100**	**10**	**100**	**10**
		90	**10**	**90**	**10**
		–	–	80	10
		70	**10**	**70**	**10**
		–	–	60	10
		–	–	–	–
		–	–	40	10
		–	–	10	100
		10	**150**	**10**	**150**
1 4 5	VTEFQ GFTWGVAGY AFAMVGKLAE	90	50	–	–
		100	50	–	–
		80	10	–	–
		70	10	–	–
		–	–	10	100
		10	**150**	**10**	**150**
		–	–	10	200

to the peptide solution enhanced solution hydrophobicity favoring sample deposition. Under these conditions, deposition of the peptide mix was feasible on all the surfaces independently of their contact angle.

3.2.2 | D/I efficiency

Having defined proper conditions to prepare samples for easy deposition on any steel plate substrates, the next optimization step was dealing with the selection of the best surfaces in terms of D/I efficiency which was determined according to the areas, intensities and signal-to-noise ratios for each of the singly charged peptide ion signals recorded in the SALDI mass spectra. Those experiments were made according two different acquisition modes ("Custom" and "MS Dried Droplet"), each with five additions of 1000 spectra. Figure 3 shows the results obtained with the MS Dried Droplet acquisition mode for steel plate #1 (left-hand column) and for steel plate #2 (right-hand column). Those results present the features of each of the 100 prepared surfaces as a function of the areas obtained for the mass spectra for the ten peptides present in the reference mixture. Figure 3A shows the results for the complete peptide mix. Figures 3B and 3C display the results for the peptides of the mixture bearing a lysine or an arginine at their C-terminal position (peptides 2 and 9, then peptides 6, 7 and 10) whereas Figure 3D refers to the other peptides of the mixture (peptides 1, 4 and 5). Green highlighting on the graphs corresponds to the surfaces showing the greatest efficiency for each group of selected peptides. As we can see from

the left-hand column, only three surfaces of steel plate #1 allowed D/I of the peptide mix. Moreover, only eight of ten peptides of the mixture were identified since peptides 3 and 8 were not detected. Similarly, recorded intensities and signal-to-noise ratio (data not shown) provided identical results to area measurements. Hence, the three selected surfaces belonging to steel plate #1 corresponded to those with the laser writing parameters of power P and frequency F equal to P80×F100, P60×F150 and P40×F150. Although surfaces from steel plate #2 allowed the identification of all ten peptides present in the mix, the selection of the best ones according to the defined performance criteria was not obvious. An additional decision item was thus implemented by considering the signal area value establishing a detection threshold to categorize peptides from the most responsive against the less efficient ones. Despite the fact that Figure 3A(#2) showed no distinctive surfaces, Figures 3B(#2) to 3D (#2) were successfully exploited under these conditions. With those criteria, six surfaces of interest with minimum area of 2×10^5 units for the two most intense peptides were evidenced from Figure 3B(#2) whereas Figures 3C(#2) and 3D(#2) led to the selection of four and five surfaces of interest, respectively, based on signal areas of 1.75×10^4 and 5×10^3 units. Moreover, and to be certain of the surface selection, these results were compared with those obtained using the "Custom" acquisition mode (see Figure S2 of the supporting information). Table 2 summarizes the selected surfaces from both acquisition modes. Despite some discrepancies observed with surfaces exhibiting good performances solely in one mode, consistent behavior was nevertheless retrieved for each studied peptide group for the surfaces indicated in bold in Table 2.

Consequently, three surfaces are selected for peptides 2 and 9 (P100×F10/P70×F10/P10×F150), four surfaces for peptides 6, 7 and 10 (P100×F10/P90×F10/P70×F10/P10×F150) and one surface for peptides 1, 4 and 5 (P10×F150). Considering that each selected surface according to the signal area was found optimal for the detection of some peptides and totally useless for others (for instance, P100×F10/P70×F10/P10×F150 suitable for peptides 2, 6, 7, 9 and 10 and not for sequences 1, 4 and 5), further evaluation was then made according to D/I efficiency of the whole sample (10 peptides) as depicted in Scheme 1. To do so, the results of the four combined graphs were considered. Three surfaces allowing the optimal D/I of the greatest number of peptides were determined. Theses surfaces were chosen according to the number of peptides they allowed to desorb and ionize efficiently by combining results from Custom and MS Dried Droplet mode. Selected surfaces from steel plate #2 were those with the following writing laser parameters of power P and frequency F: P100×F10 (5 peptides) and P70×F10/P10×F150 (8 peptides).

3.2.3 | Deposition homogeneity

Nevertheless, the selection of the optimal steel plate surfaces based on the D/I effectiveness must be complemented since this criterion

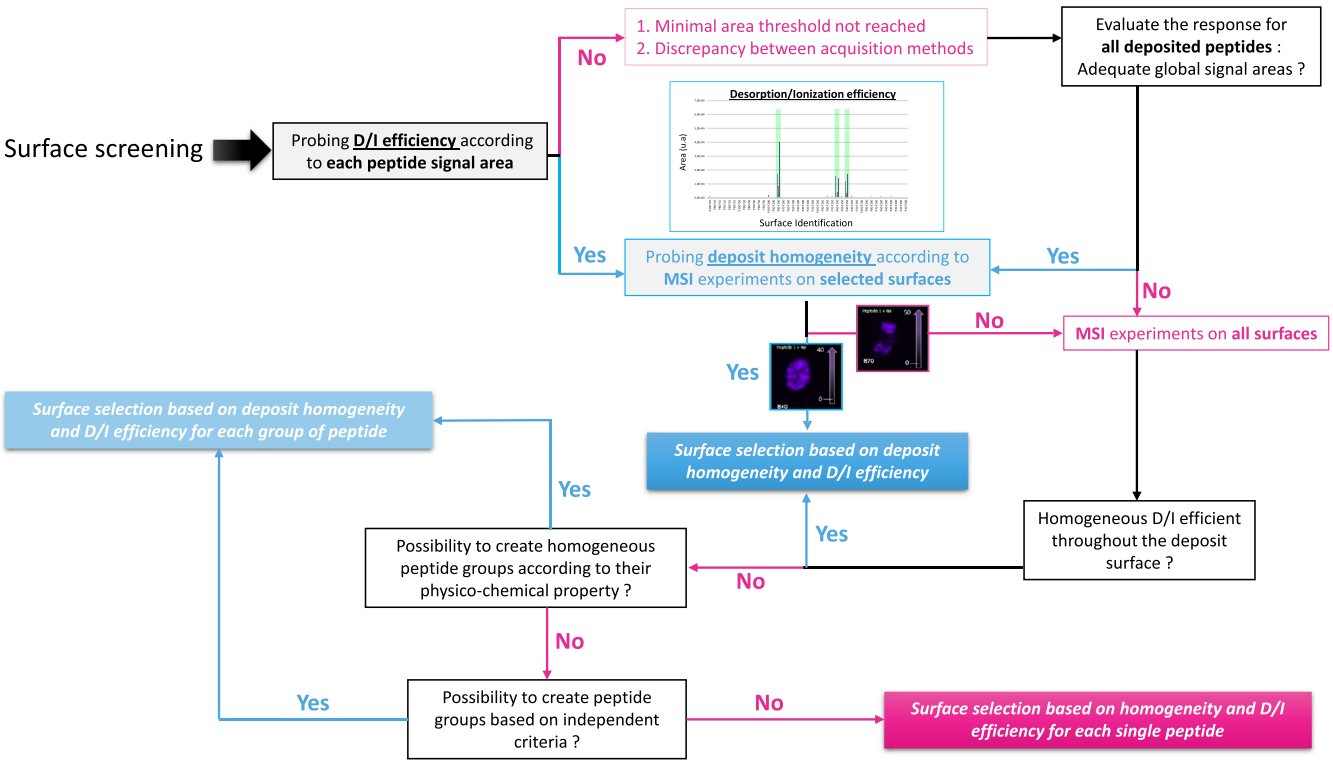

SCHEME 1 Hierarchical decision tree to choose the best surface according to D/I efficiency and deposit homogeneity [Color figure can be viewed at wileyonlinelibrary.com]

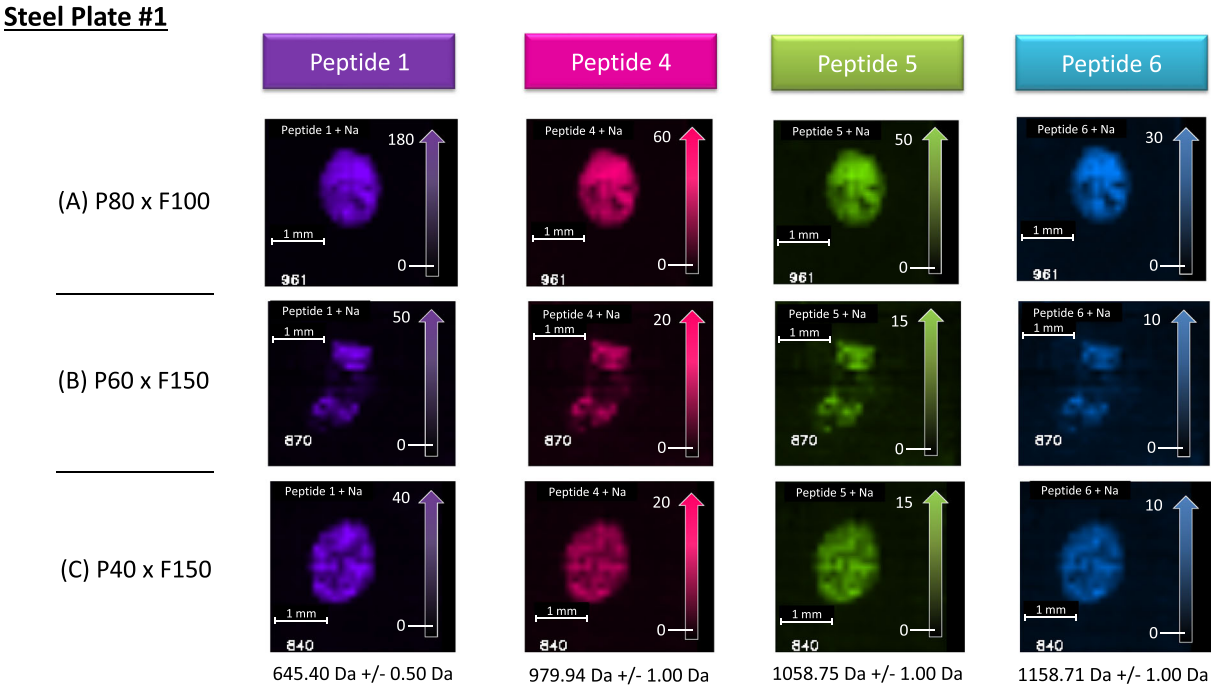

FIGURE 4 SALDI-MSI ionic images for steel plate #1 of peptides 1, 4, 5 and 6 recorded in positive mode for surfaces (A) P80×F100; (B) P60×F150; (C) P40×F150 [Color figure can be viewed at wileyonlinelibrary.com]

alone cannot be used on its own without taking into account that the prepared surfaces must also enable homogeneous deposition of the peptide mixture. As previously mentioned, one of the major drawbacks of MALDI approaches is the recourse to organic matrices that may lead to various sample surface heterogeneity (coffee stain effect/hot spot) appearing upon deposit drying. When using SALDI substrates, we could think that, without co-crystallization with an organic matrix, this effect would be eliminated. Unfortunately, this was not the case since the solvent evaporation process from a deposited droplet affected analyte partitioning on the steel plates. The contact line between droplets and some of the prepared steel surfaces remained pinned during the drying step. The droplet then caved in through the process leading to a constant change in contact angle explaining the transport of particles to the edge of the droplet that is responsible for the coffee stain effect.[50–52] Of note, the homogeneity of the deposit is a major concern in SALDI-MS. While in-source camera allows visual inspection of deposits in MALDI-MS with non-homogeneous analyte/matrix repartition easily recognizable, deposits in SALDI-MS devoid of large quantities of matrices are not discernable with the naked eye nor with the in-source camera. In the case of non-homogeneous deposits, finding the position of the analyte of interest within hot spots or at the periphery (coffee stain effect) is almost impossible on SALDI substrates. In particular, if we do not know where to direct the laser, whatever the irradiation pathway method, the lack of a feature signal in a recorded SALDI mass spectrum may be due to the real absence of the analyte or to an error on the localization of the laser impingement zone. To overcome this issue, we designed an optimized laser acquisition pattern as described previously, and we addressed the physicochemical properties of the prepared steel substrates towards their ability to lead to homogeneous deposits, the most important parameter ensuring acquisition reliability. For that purpose, MSI analyses were carried out on the SALDI steel plates according to two types of experiments with the peptide mix. According to the hierarchical decision tree depicted in Scheme 1, only the surfaces of steel plate #1 having been considered as optimal with the criterion of D/I effectiveness (surfaces P80×F100, P60×F150 and P40×F150) were subjected to MSI experiment (Figure 4). The results are presented for four peptides from the mix (1, 4, 5 and 6) which are the most representative ones producing sodiated ions ($[M + Na]^+$ selected for MSI analyses: *m/z* 645.40 Da (peptide 1), *m/z* 979.94 Da (peptide 4), *m/z* 1058.75 Da (peptide 5) and *m/z* 1158.71 Da (peptide 6)). Results are presented according to a colorimetric scale for each peptide (peptide 1 in violet, 4 in pink, 5 in green and 6 in blue). For the P80×F100 and the P40×150 surfaces, the four peptides were deposited homogeneously whereas the P60×F150 surface showed non-homogeneous peptide repartition. Two areas appeared as highlighted while the center was completely dark corresponding to absence of the expected ions. Therefore, this surface was finally not selected for further experiments. Other peptides from the mix behaved the same in MSI experiments as the presented ones (data not shown). Thus, P80×F100 and P40×F150 surfaces were selected as optimal surfaces for steel plate #1 because they combined D/I efficiency and homogeneity criteria. In contrast, 50 surfaces of steel plate #2 were subjected to MSI experiments with the peptide mix since the D/I performance of such substrates was difficult to evaluate as previously discussed. To determine the best steel plate #2 surfaces according to deposit homogeneity, a focus on MSI experiment

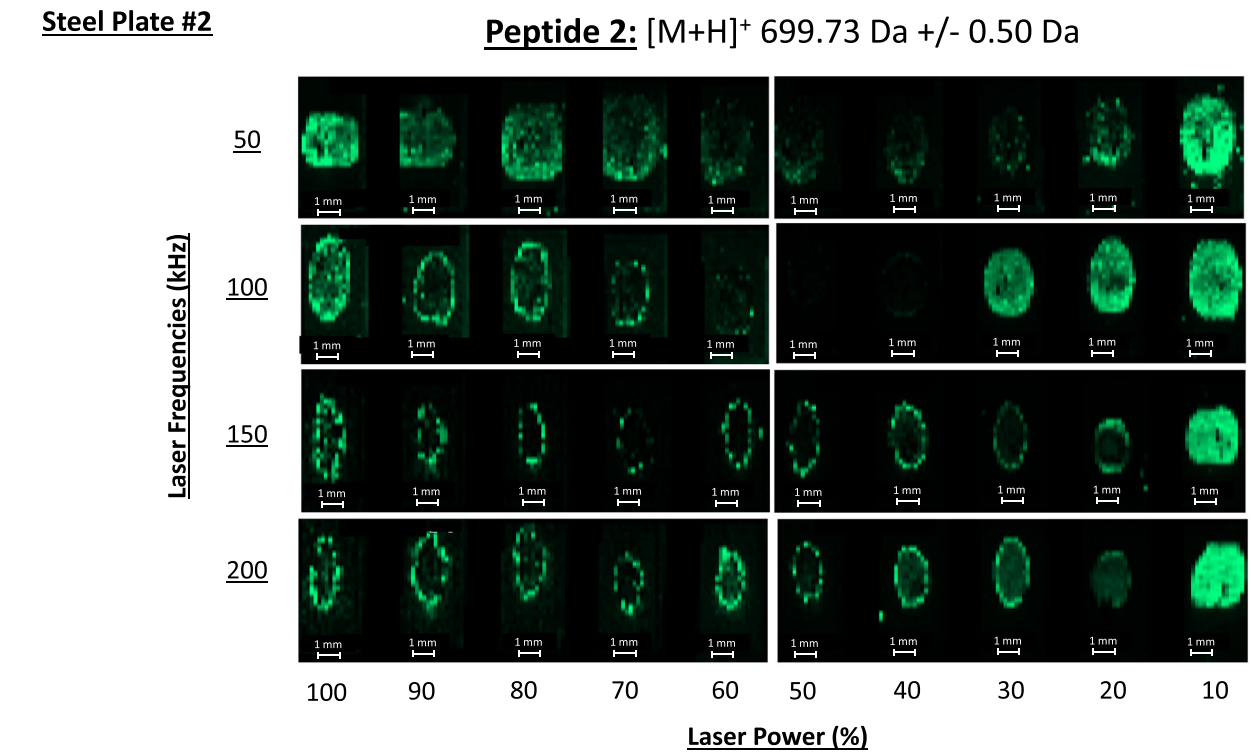

FIGURE 5 SALDI-MSI ionic images for steel plate #2 of peptide 2 recorded in positive mode. Ionic images are presented for analysis with laser frequencies ranging from 50 to 200 kHz and laser power ranging from 10% to 100% [Color figure can be viewed at wileyonlinelibrary.com]

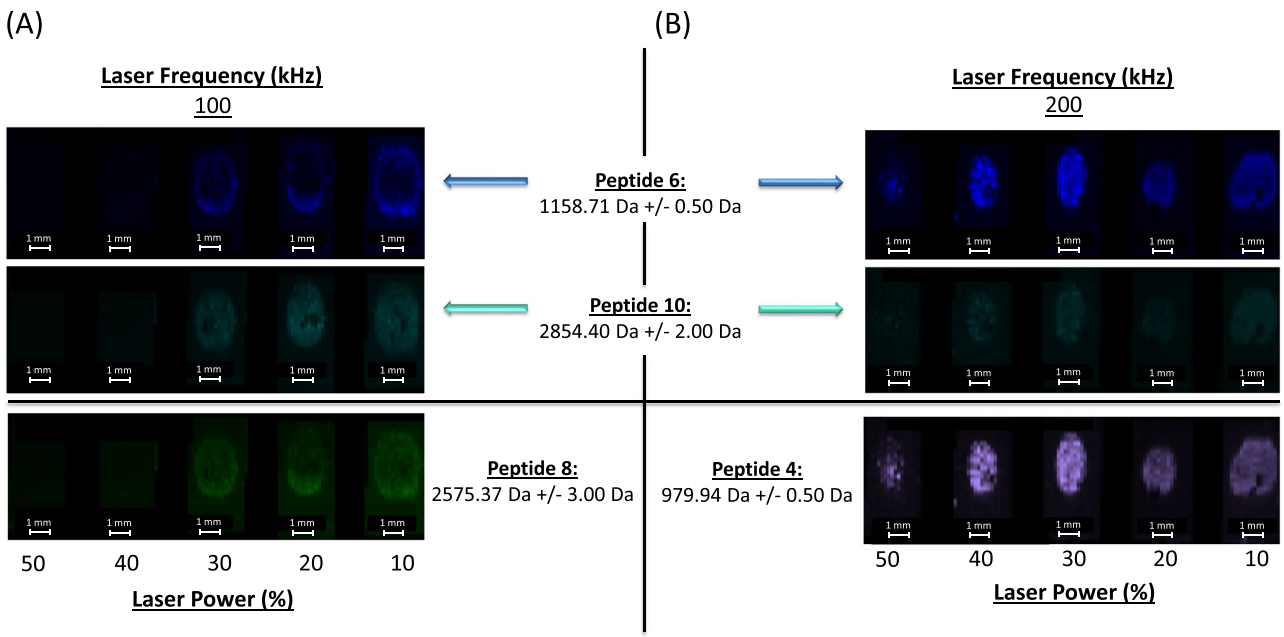

FIGURE 6 SALDI-MSI ionic images for steel plate #2 of peptides 4, 6, 8 and 10. Ionic images are presented for analysis with laser frequencies of (A) 100 kHz and (B) 200 kHz and laser power ranging from 10% to 50% [Color figure can be viewed at wileyonlinelibrary.com]

conducted on peptide 2 ($[M + H]^+$: m/z 699.73 Da) was first undertaken (Figure 5). Ionic images were acquired for 40 of the 50 surfaces of steel plate #2 since the surfaces with a writing laser frequency of 10 kHz did not allow any signal. Figure 5 displays ionic images of peptide 2 following a decreasing laser power ranging from 100% to 10% and for increasing laser frequencies ranging from 50 to 200 kHz shown respectively from left to right and from top to bottom. A green colorimetric scale is used to identify the presence of

the targeted peptide ($[M + H]^+$ at *m/z* 699.73 Da). Only 6 of the 40 surfaces allowed a homogeneous deposition of the selected peptide as long as the laser writing power was established at 10% whatever the frequency settings (F50×P10; F100×P10; F150×P10; F200×P10). For the specific laser frequency of 100 kHz, laser power of 10% as stated but also of 20% as well as 30% were also optimal (F100×P30; F100×P20). Those six surfaces were found also appropriate for peptide 9 (*m/z* 2636.21 Da) (data not shown). To ascertain surface selection, other peptides from the mix were imaged. Figure 6 presents the results obtained for surfaces made with writing laser frequencies of 100 kHz (Figure 6A) and 200 kHz (Figure 6B) and laser powers ranging from 10% to 50%. Figure 6A shows ionic images of *m/z* 1158.71 Da ($[M + Na]^+$ of peptide 6), *m/z* 2575.37 Da ($[M + H]^+$ of peptide 8) and *m/z* 2854.40 Da ($[M + H]^+$ of peptide 10). In Figure 6B, the same peptides are represented except for peptide 8 which is replaced by *m/z* 979.94 Da ($[M + Na]^+$ of peptide 4). Peptides 6 and 10 were detected and observed with surfaces prepared with writing laser frequency of 100 kHz and writing laser powers of 10% to 30% or with frequency of 200 kHz and powers of 10% to 50%. Additionally, peptide 4 was only detected with surfaces with a writing laser frequency of 200 kHz and writing laser powers of 10–50%. Similarly, images of peptide 8 were only obtained for surfaces with a writing laser frequency of 100 kHz and writing laser powers of 10% to 30%. According to these results, the performance of the steel plate #2 surfaces towards homogeneous peptide distribution clearly depended on peptide physicochemical parameters. Indeed, according to the six selected peptides, only three surfaces (P30×F100; P20×F100; P10×F100) enabled homogeneous depositions. But, when we moved to another set of four peptides (4, 6, 7 and 10), different optimal writing parameters were defined (laser power and frequencies of P40×F200 and P30×F200). Given the discrepancy of the results, only the five surfaces, with frequencies of 100 and 200 kHz, previously presented were finally selected as optimal considering that, despite the fact that each steel plate surface can be more efficient for specific sequences, they were overall quite efficient for a majority of the peptides from the mix.

3.3 | MALDI-MS and SALDI-MS analyses for the two most appropriate steel plates

To compare steel-plate-mediated SALDI analyses with the reference MALDI technology within the frame of peptide detection, two of the surfaces that had been categorized as optimal were selected: one from plate #1 (P80×F100) and one from plate #2 (P10×F100). Figure 7 presents the mass spectra obtained for the analysis of the reference mixture on plate #1 P80×F100 (Figure 7A) and plate #2

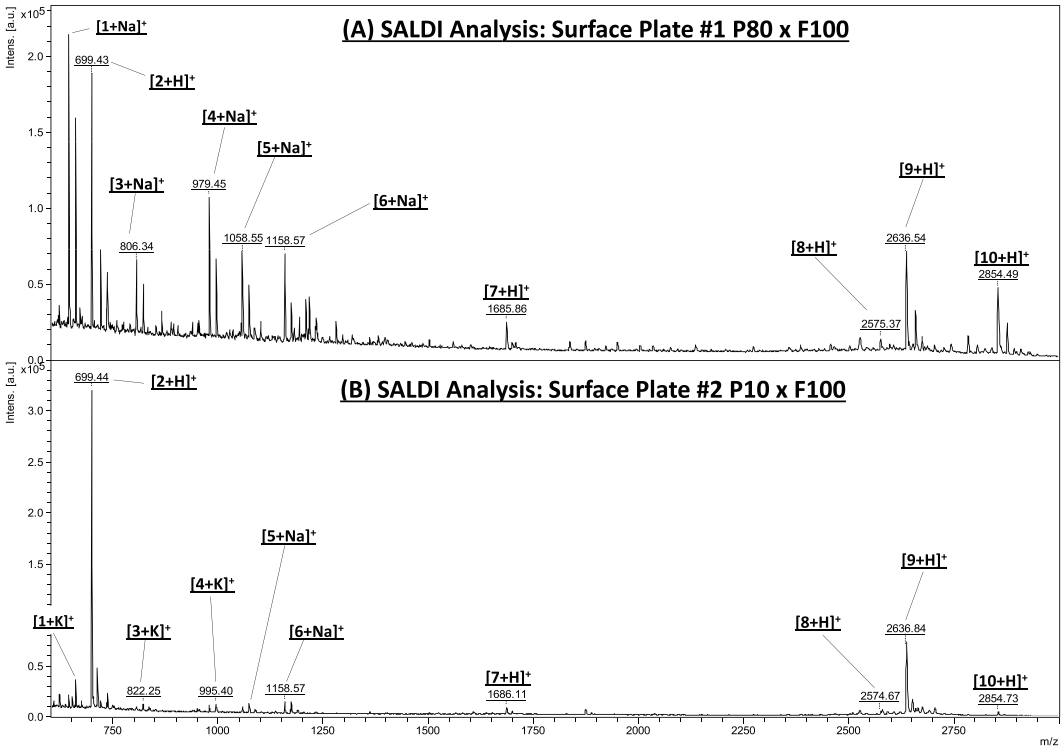

Peptide	Area (u.a)	Intensity (u.a)	S/N
1	65110	372932	63
2	51554	308585	43
3	21218	110712	18
4	36092	173606	38
5	23913	116609	26
6	25818	107025	27
7	8480	25082	19
8	5751	13711	11
9	82040	112911	41
10	60476	70236	44

"MS Dried Droplet" mode with five addition of 1000 spectra

Peptide	Area (u.a)	Intensity (u.a)	S/N
1	20162	81366	28
2	151548	357136	242
3	1998	12198	11
4	8237	23097	14
5	9168	22058	15
6	15706	27457	22
7	8455	8932	17
8	3264	4175	9
9	214664	83302	118
10	10683	4199	17

FIGURE 7 SALDI-MS spectra of the reference peptide mix recorded in positive mode with 90% laser fluence, MS Dried Droplet acquisition mode and accumulation of 1000 spectra instead of 300 on (A) steel plate #1/surface P80×F100 and (B) steel plate #2/surface P10×F100 [Color figure can be viewed at wileyonlinelibrary.com]

P10×F100 (Figure 7B). All the peptides from the mix were detected and identified with both surfaces. Another important fact was that peptides were present in the spectra in three predominant adduct forms: H^+, Na^+ and K^+. To precisely compare both surfaces, all adducts in the spectra were considered. According to ratios between plate #1 and plate #2 of area, ion intensity and signal-to-noise ratio (see Table S3 of the supporting information), eight peptides seemed to be better desorbed and ionized with surface P80×F100 (plate #1) which had undergone a hatching with one passage of the writing laser. This difference shows the increase in the efficiency of the surfaces in terms of D/I of the peptides. Thus, fewer laser passes allow better adsorption of compounds and increases the efficiency of the analysis. Moreover, when comparing these results with MALDI-MS ones, six peptides from the mix were more efficiently detected by the developed SALDI method than by classical MALDI. Last but not least, both SALDI surfaces allowed the identification of a supplementary peptide (peptide 9, *m/z* 2636.39 Da) that optimized MALDI-MS failed to detect demonstrating the significance of the prepared steel plates.

4 | CONCLUSIONS

Different steel plate textured surfaces were tested and several of them were selected as adequate according to two criteria: the efficiency of D/I and the homogeneity of the deposits. The results obtained showed that the use of SALDI steel plates proved more efficient than conventional MALDI analysis for peptide analyses, especially because the homogeneity of the deposits using steel plate optimal surfaces was much better than with organic matrices. The combined use of these two techniques could improve the efficiency and repeatability of peptide analyses using LDI-MS.

ACKNOWLEDGEMENTS

The authors thank Dr. L. Mouls and Dr. N. Shenar for peptide synthesis and purification. The authors acknowledge the Agence Nationale de la Recherche (ANR) for financial support as part of the ANR NanoIntra project (ANR-19-CE09-0030), the Centre National de la Recherche Scientifique (CNRS), the University of Lille and the University of Montpellier. The authors also acknowledge the LEAF platform: Laser processing platform for multifunctional electronics on Flex (ANR-11-EQUIPEX-0025). This work was partly supported by the French RENATECH network (French national nanofabrication platform).

DATA AVAILABILITY STATEMENT

Data available on request from the authors.

PEER REVIEW

The peer review history for this article is available at https://publons.com/publon/10.1002/rcm.9476.

ORCID

Claudia Bich https://orcid.org/0000-0002-8243-4018

REFERENCES

1. Fenner NC, Daly NR. Laser used for mass analysis. *Rev Sci Instrum*. 1966;37(8):1068-1070. doi:10.1063/1.1720410
2. Vastola FJ, Mumma RO, Pirone AJ. Analysis of organic salts by laser ionization. *Org Mass Spectrom*. 1970;3(1):101-104. doi:10.1002/oms.1210030112
3. Karas M, Hillenkamp F. Laser desorption ionization of proteins with molecular masses exceeding 10,000 Daltons. *Anal Chem*. 1988;60(20):2299-2301. doi:10.1021/ac00171a028
4. Mandal A, Singha M, Addy PS, Basak A. Laser desorption ionization mass spectrometry: Recent progress in matrix-free and label-assisted techniques. *Mass Spectrom Rev*. 2019;38(1):3-21. doi:10.1002/mas.21545
5. Strupat K, Karas M, Hillenkamp F. 2,5-Dihydroxybenzoic acid: A new matrix for laser desorption–ionization mass spectrometry. *Int J Mass Spectrom Ion Processes*. 1991;111:89-102. doi:10.1016/0168-1176(91)85050-V
6. Karas M, Ehring H, Nordhoff E, et al. Matrix-assisted laser desorption/ionization mass spectrometry with additives to 2,5-dihydroxybenzoic acid. *Org Mass Spectrom*. 1993;28(12):1476-1481. doi:10.1002/oms.1210281219
7. Beavis RC, Chait BT, Fales HM. Cinnamic acid derivatives as matrices for ultraviolet laser desorption mass spectrometry of proteins. *Rapid Commun Mass Spectrom*. 1989;3(12):432-435. doi:10.1002/rcm.1290031207
8. Beavis RC, Chait BT. Rapid, sensitive analysis of protein mixtures by mass spectrometry. *Proc Natl Acad Sci*. 1990;87(17):6873-6877. doi:10.1073/pnas.87.17.6873
9. Mank M, Stahl B, Boehm G. 2,5-Dihydroxybenzoic acid butylamine and other ionic liquid matrixes for enhanced MALDI-MS analysis of biomolecules. *Anal Chem*. 2004;76(10):2938-2950. doi:10.1021/ac030354j
10. Reyzer ML, Caprioli RM. MALDI-MS-based imaging of small molecules and proteins in tissues. *Curr Opin Chem Biol*. 2007;11(1):29-35. doi:10.1016/j.cbpa.2006.11.035
11. König S. Target coatings and desorption surfaces in biomolecular MALDI-MS. *Proteomics*. 2008;8(4):706-714. doi:10.1002/pmic.200700782
12. Siuzdak G. An Introduction to mass spectrometry ionization: An excerpt from *The Expanding Role of Mass Spectrometry in Biotechnology*, 2nd Ed.; MCC Press: San Diego, 2005. *JALA: J Assoc Lab Autom*. 2004;9(2):50-63. doi:10.1016/j.jala.2004.01.004
13. Strathmann FG, Hoofnagle AN. Current and future applications of mass spectrometry to the clinical laboratory. *Am J Clin Pathol*. 2011;136(4):609-616. doi:10.1309/AJCPW0TA8OBBNGCK
14. Wang BH, Dreisewerd K, Bahr U, Karas M, Hillenkamp F. Gas-phase cationization and protonation of neutrals generated by matrix-assisted laser desorption. *J Am Soc Mass Spectrom*. 1993;4(5):393-398. doi:10.1016/1044-0305(93)85004-H
15. Gabriel SJ, Schwarzinger C, Schwarzinger B, Panne U, Weidner SM. Matrix segregation as the major cause for sample inhomogeneity in MALDI dried droplet spots. *J Am Soc Mass Spectrom*. 2014;25(8):1356-1363. doi:10.1007/s13361-014-0913-0
16. Garden RW, Sweedler JV. Heterogeneity within MALDI samples as revealed by mass spectrometric imaging. *Anal Chem*. 2000;72(1):30-36. doi:10.1021/ac9908997
17. Giordano S, Zucchetti M, Decio A, et al. Heterogeneity of paclitaxel distribution in different tumor models assessed by MALDI mass spectrometry imaging. *Sci Rep*. 2016;6(1):39284. doi:10.1038/srep39284

18. Longuespée R, Casadonte R, Kriegsmann M, et al. MALDI mass spectrometry imaging: A cutting-edge tool for fundamental and clinical histopathology. *Proteomics ClinAppl*. 2016;10(7):701-719. doi:10.1002/prca.201500140
19. Bien T, Koerfer K, Schwenzfeier J, Dreisewerd K, Soltwisch J. Mass spectrometry imaging to explore molecular heterogeneity in cell culture. *Proc Natl Acad Sci*. 2022;119(29):e2114365119. doi:10.1073/pnas.2114365119
20. Sunner J, Dratz E, Chen YC. Graphite surface-assisted laser desorption/ionization time-of-flight mass spectrometry of peptides and proteins from liquid solutions. *Anal Chem*. 1995;67(23):4335-4342. doi:10.1021/ac00119a021
21. Tanaka K, Waki H, Ido Y, et al. Protein and polymer analyses up to m/z 100 000 by laser ionization time-of-flight mass spectrometry. *Rapid Commun Mass Spectrom*. 1988;2(8):151-153. doi:10.1002/rcm.1290020802
22. Dattelbaum AM, Iyer S. Surface-assisted laser desorption/ionization mass spectrometry. *Expert Rev Proteomics*. 2006;3(1):153-161. doi:10.1586/14789450.3.1.153
23. Kuzema PA. Small-molecule analysis by surface-assisted laser desorption/ionization mass spectrometry. *J Anal Chem*. 2011;66(13):1227-1242. doi:10.1134/S1061934811130065
24. Northen TR, Woo H-K, Northen MT, et al. High surface area of porous silicon drives desorption of intact molecules. *J Am Soc Mass Spectrom*. 2007;18(11):1945-1949. doi:10.1016/j.jasms.2007.08.009
25. Hansen RL, Dueñas ME, Lee YJ. Sputter-coated metal screening for small molecule analysis and high-spatial resolution imaging in laser desorption ionization mass spectrometry. *J Am Soc Mass Spectrom*. 2019;30(2):299-308. doi:10.1007/s13361-018-2081-0
26. Abdelhamid HN. Nanoparticle assisted laser desorption/ionization mass spectrometry for small molecule analytes. *Microchimica Acta*. 2018;185(3):200. doi:10.1007/s00604-018-2687-8
27. Yagnik GB, Hansen RL, Korte AR, Reichert MD, Vela J, Lee YJ. Large scale nanoparticle screening for small molecule analysis in laser desorption ionization mass spectrometry. *Anal Chem*. 2016;88(18):8926-8930. doi:10.1021/acs.analchem.6b02732
28. Pilolli R, Palmisano F, Cioffi N. Gold nanomaterials as a new tool for bioanalytical applications of laser desorption ionization mass spectrometry. *Anal Bioanal Chem*. 2012;402(2):601-623. doi:10.1007/s00216-011-5120-2
29. Zhu Q, Wang Z, Wang Y, et al. Investigation of surface morphology on ion desorption in SALDI-MS on tailored silicon nanopillar arrays. *J Phys Chem C*. 2020;124(4):2450-2457. doi:10.1021/acs.jpcc.9b09520
30. Law KP. Laser desorption/ionization mass spectrometry on nanostructured semiconductor substrates: DIOS™ and QuickMass™. *Int J Mass Spectrom*. 2010;290(2):72-84. doi:10.1016/j.ijms.2009.12.006
31. Xiao Y, Retterer ST, Thomas DK, Tao J-Y, He L. Impacts of surface morphology on ion desorption and ionization in desorption ionization on porous silicon (DIOS) mass spectrometry. *J Phys Chem C*. 2009;113(8):3076-3083. doi:10.1021/jp808844f
32. Schulz S, Becker M, Groseclose MR, Schadt S, Hopf C. Advanced MALDI mass spectrometry imaging in pharmaceutical research and drug development. *Curr Opin Biotechnol*. 2019;55:51-59. doi:10.1016/j.copbio.2018.08.003
33. Swales JG, Hamm G, Clench MR, Goodwin RJA. Mass spectrometry imaging and its application in pharmaceutical research and development: A concise review. *Int J Mass Spectrom*. 2019;437:99-112. doi:10.1016/j.ijms.2018.02.007
34. Qiao L, Liu B, Girault HH. Nanomaterial-assisted laser desorption ionization for mass spectrometry-based biomedical analysis. *Nanomedicine*. 2010;5(10):1641-1652. doi:10.2217/nnm.10.127
35. Schwamborn K, Kriegsmann M, Weichert W. MALDI imaging mass spectrometry – From bench to bedside. *Biochim Biophys Acta (BBA)*. 2017;1865(7):776-783. doi:10.1016/j.bbapap.2016.10.014
36. Cornett DS, Reyzer ML, Chaurand P, Caprioli RM. MALDI imaging mass spectrometry: Molecular snapshots of biochemical systems. *Nat Methods*. 2007;4(10):828-833. doi:10.1038/nmeth1094
37. Lagarrigue M, Caprioli RM, Pineau C. Potential of MALDI imaging for the toxicological evaluation of environmental pollutants. *J Proteomics*. 2016;144:133-139. doi:10.1016/j.jprot.2016.05.008
38. Guinan T, Kirkbride P, Pigou PE, Ronci M, Kobus H, Voelcker NH. Surface-assisted laser desorption ionization mass spectrometry techniques for application in forensics. *Mass Spectrom Rev*. 2015;34(6):627-640. doi:10.1002/mas.21431
39. Kraj A, Świst M, Strugala A, Parczewski A, Silberringa J. Fingerprinting of 3,4-methylenedioxymethamphetamine markers by desorption/ionization on porous silicon. *Eur J Mass Spectrom*. 2006;12(4):253-259. doi:10.1255/ejms.811
40. Amin MO, Al-Hetlani E. Development of efficient SALDI substrate based on Au–TiO_2 nanohybrids for environmental and forensic detection of dyes and NSAIDs. *Talanta*. 2021;233:122530. doi:10.1016/j.talanta.2021.122530
41. Guinan, T. M, Kirkbride P, Vedova CBD, Kershaw, S. G, Kobus H, Voelcker, N. H. Direct detection of illicit drugs from biological fluids by desorption/ionization mass spectrometry with nanoporous silicon microparticles. *Analyst*. 2015;140(23):7926-7933. doi:10.1039/C5AN01754H
42. Shi R, Dai X, Li W, et al. Hydroxyl-group-dominated graphite dots reshape laser desorption/ionization mass spectrometry for small biomolecular analysis and imaging. *ACS Nano*. 2017;11(9):9500-9513. doi:10.1021/acsnano.7b05328
43. Mouls L, Subra G, Aubagnac J-L, Martinez J, Enjalbal C. Tandem mass spectrometry of amidated peptides. *J Mass Spectrom*. 2006;41(11):1470-1483. doi:10.1002/jms.1118
44. Dupré M, Cantel S, Martinez J, Enjalbal C. Occurrence of C-terminal residue exclusion in peptide fragmentation by ESI and MALDI tandem mass spectrometry. *J Am Soc Mass Spectrom*. 2012;23(2):330-346. doi:10.1007/s13361-011-0254-1
45. Dreisewerd K. Recent methodological advances in MALDI mass spectrometry. *Anal Bioanal Chem*. 2014;406(9):2261-2278. doi:10.1007/s00216-014-7646-6
46. Qiao Z, Lissel F. MALDI matrices for the analysis of low molecular weight compounds: Rational design, challenges and perspectives. *Chem Asian J*. 2021;16(8):868-878. doi:10.1002/asia.202100044
47. Marsico ALM, Duncan B, Landis RF, Tonga GY, Rotello VM, Vachet RW. Enhanced laser desorption/ionization mass spectrometric detection of biomolecules using gold nanoparticles, matrix, and the coffee ring effect. *Anal Chem*. 2017;89(5):3009-3014. doi:10.1021/acs.analchem.6b04538
48. Gabriel SJ, Pfeifer D, Schwarzinger C, Panne U, Weidner SM. Matrix-assisted laser desorption/ionization time-of-flight mass spectrometric imaging of synthetic polymer sample spots prepared using ionic liquid matrices. *Rapid Commun Mass Spectrom*. 2014;28(5):489-498. doi:10.1002/rcm.6810
49. Hu J-B, Chen Y-C, Urban PL. Coffee-ring effects in laser desorption/ionization mass spectrometry. *Anal Chim Acta*. 2013;766:77-82. doi:10.1016/j.aca.2012.12.044
50. Kudina O, Eral B, Mugele F. E-MALDI: An Electrowetting-enhanced drop drying method for MALDI mass spectrometry. *Anal Chem*. 2016;88(9):4669-4675. doi:10.1021/acs.analchem.5b04283
51. Zang D, Tarafdar S, Tarasevich YY, Dutta Choudhury M, Dutta T. Evaporation of a droplet: From physics to applications. *Phys Rep*. 2019;804:1-56. doi:10.1016/j.physrep.2019.01.008

52. Yunker PJ, Still T, Lohr MA, Yodh AG. Suppression of the coffee-ring effect by shape-dependent capillary interactions. *Nature*. 2011; 476(7360):308-311. doi:10.1038/nature10344

SUPPORTING INFORMATION

Additional supporting information can be found online in the Supporting Information section at the end of this article.

How to cite this article: Cournut A, Hosu IS, Braud F, et al. Development of nanomaterial enabling highly sensitive surface-assisted laser desorption/ionization mass spectrometry peptide analysis. *Rapid Commun Mass Spectrom*. 2023;37(8):e9476. doi:10.1002/rcm.9476